

ORIGINAL RESEARCH

Design of Capacitive Electrostatic Probes for Online Measurement of Surface Charge on Tri-post Insulators

Jiayi Liu¹, Xiaoqing Xie¹, Feng Wang¹ , She Chen¹, Qiuqin Sun¹, Lipeng Zhong¹, Xianhao Fan², Fangwei Liang² 

¹College of Electrical and Information Engineering, Hunan University, Changsha 410082, China

²Department of Electrical Engineering, Tsinghua University, Beijing 100084, China

Correspondence

Feng Wang: wangfeng55@263.net

Fangwei Liang: liangfangwei@tsinghua.edu.cn

Funding information

National Natural Science Foundation of China under Grant 52237007 and 52377143, and the Natural Science Foundation of Hunan Province under Grant 2022JJ20010.

Abstract

Compared to offline measurement (interrupting the applied voltage before measurement), online measurement of surface charge on gas-insulated transmission line (GIL) insulators effectively avoids the impact of spontaneous dissipation of charges. Thus, the accuracy of results can be improved. In this paper, a measurement model of capacitive electrostatic probes for surface charges on ± 320 kV GIL tri-post insulator is established. The geometry of probes is optimized. The feasibility of online measurement of surface charges is analyzed. Results indicate that the surface leakage distance of induced charges is positively related to the length. Furthermore, as the diameter of probes increases, the maximum electric field on the sensitive electrode surface rises, while the radius of the sensitive electrode has the opposite effect. Hence, the diameter of the probe is 6 mm. The length and radius of sensitive electrodes are 50 mm and 1.2 mm, respectively. For online measurement of surface charges on ± 320 kV tri-post insulators, the induced potential distribution of the probe is consistent with surface charges. Therefore, the capacitive electrostatic probe in the embedded electrode is appropriate for the online measurement of surface charges on tri-post insulators. It provides a reference for avoiding flashover triggered by surface charge accumulation on DC GIL insulators.

1 INTRODUCTION

Al_2O_3 /epoxy resin insulators, such as tri-post and basin insulators, are essential components of the DC GIL. They provide support for high voltage conductors and ensure the insulation gap between the conductor and the grounded enclosure [1–3]. For composite insulation systems constructed by insulators and SF_6 or SF_6/N_2 gas mixtures, surface flashover of the gas-solid interface significantly reduces the insulation strength [4–6]. This is because the electric field distribution of insulators is inevitably affected by surface charges [7–9]. Hence, the measurement of surface charges has received widespread attention. In general, the distribution of the insulator surface potential is obtained by electrostatic probes after disconnecting the operation voltage (i.e., offline measurement). The inversion algorithm can then calculate the surface charge density [10–12]. However, charge dissipation is unavoidable during the offline measurement. Thus, the accuracy of results decreases. Furthermore, the surface flashover generates a significant quantity of charged particles that easily migrate to the insulator surface. This may result in measurement deviations when combined with heteropolar surface charges [13]. Therefore, it is necessary to carry out surface charge measurement under online conditions to reveal the mechanism of flashover triggered by surface charges.

The surface charge measurement primarily relies on Kelvin electrostatic probes and capacitive electrostatic probes [14,15]. The Kelvin electrostatic probe is based on the principle of electric field compensation [16,17]. It is an active probe connected to a high voltage power source, with its potential continuously adjusting until it matches the potential on the sample. When the two potentials are equal, the induced current through the probe becomes zero and is unaffected by the capacitance between probes and samples [18,19]. The surface potential of insulators can be quantitatively measured by Kelvin electrostatic probes. Typical products include Trek 347, Trek 3455ET, and Monroe 1017AE [20–22]. During the measurement, the gap between the probe and the sample is approximately 3 mm [23–25]. The effective aperture of the probe input end is 1.78 mm. The spatial resolution is a circular area with a diameter of about 7 mm. Besides, the voltage resolution is ± 1 V [26], and the response time for the 1 kV step voltage is lower than 3 ms [27]. Therefore, Kelvin probes are widely used for surface charge measurements of insulators due to their higher spatial resolution, response speed, and accuracy.

Unlike Kelvin electrostatic probes, capacitive electrostatic probes measure the surface charge following the principle of electrostatic induction, as proposed by D. K. Davies *et al.* in 1967 [28,29]. When the sensitive electrode approaches the charged surface of the material, a certain induced potential is generated. According to the principle of the capacitive voltage

division, it is possible to determine the charge density by collecting the induced potential [30,31]. However, the induced potential of probes is influenced by the charge around the measured surface. Therefore, Faircloth *et al.* proposed the φ function method for inverse calculation of charge density distribution by considering the overall surface potential distribution of insulators, thus improving the measurement accuracy [32,33]. Moreover, there is an inevitable leakage of induced charges on sensitive electrodes. The main leakage pathway includes: through the insulator body, along the insulator surface, and through the operational amplifier pins of the collection unit. Therefore, many methods are successively adopted to improve the leakage time constant of induced charges, thereby ensuring measurement accuracy. The methods include extending the surface leakage distance of insulators, increasing the grounded distance of operational amplifier pins, and designing shielding structures [34,35]. For example, Wang *et al.* used the AD 549LH operational amplifier with high input impedance and low leakage current to build the acquisition unit for the electrostatic probe [36]. Thus, the leakage time constant of the induced charge is increased to 2000 seconds. It is inferred that the charge density can be evaluated based on the induced potential collected by the electrostatic probe. Capacitive electrostatic probes are still used for offline measurements after the applied voltage is disconnected due to the limitation of the measurement range. However, there is still a lack of online measurement methods for surface charges of DC GIL insulators.

In this paper, an online measurement model of the capacitive electrostatic probe is presented to assess the surface charge distribution of tri-post insulators. The impact of the diameter of the probe, the radius, and the length of the sensitive electrode on the induced potential, the electric field distribution, and the spatial resolution are studied. The geometry of the probe is optimized for online measurement. For the $\pm 320\text{kV}$ GIL tri-post insulator, the electric field before and after the electrostatic probe arrangement in the embedded electrode is compared. The spatial resolution of probes for online measurement is discussed. The feasibility of capacitive electrostatic probes for online measurement of surface charges on tri-post insulators is verified.

2 MEASUREMENT PRINCIPLE OF CAPACITIVE ELECTROSTATIC PROBE

Fig. 1 depicts the geometric structure of the capacitive electrostatic probe, which is cylindrical [35,36]. The sensitive electrode is secured at the center of the probe by a high resistance insulation material. Additionally, the shell of the probe is grounded to shield the impact of external electric fields. A certain induced potential is generated by the probe based on electrostatic induction. Fig. 1(b) depicts the equivalent circuit of the probe. Q represents the number of charges on the measured surface. U_0 is the induced potential of probes. The capacitance between probes and samples is C_s . The capacitance of the sample and the sensitive electrode to the ground are C_d and C_e , respectively.

According to the principle of capacitive voltage division:

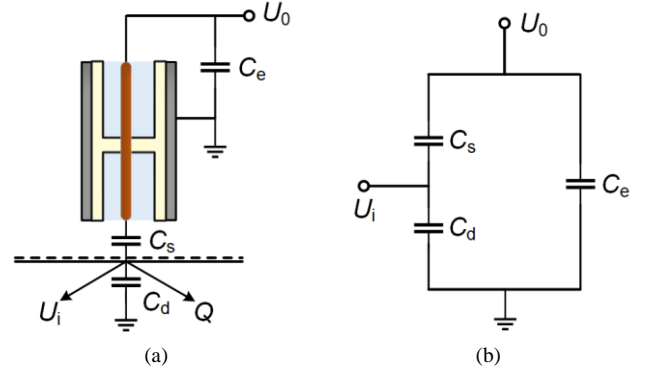


Fig. 1. Diagram of capacitive electrostatic probes. (a) Geometric structure; (b) Equivalent circuit.

$$U_0 = \frac{C_s}{C_s + C_e} \cdot U_i \quad (1)$$

$$Q = \sigma \cdot S \quad (2)$$

where σ is the surface charge density. U_i represents the surface potential of samples, while S is the effective charged area. The relationship between U_0 and S is as follows:

$$U_0 = \frac{C_s \cdot S \cdot \sigma}{C_s C_e + C_s C_d + C_e C_d} \quad (3)$$

It can be obtained from (3):

$$\sigma = M \cdot U_0 \quad (4)$$

$$M = \frac{C_e}{S} \cdot \left(1 + \frac{C_d}{C_e} + \frac{C_d}{C_s}\right) \quad (5)$$

where M is the scale coefficient. When $C_d \ll C_s \ll C_e$, then, $M \approx C_e/S$.

In order to calibrate the response characteristics of capacitive electrostatic probes, a specific DC voltage is given to the metal plate electrode. The electrostatic probe and the plate electrode are vertically positioned, with a distance of approximately 3mm. The linear relationship between U_i and U_0 is obtained by increasing the voltage step by step, expressed as $U_0 = aU_i + b$. After measuring the grounded capacitance C_e of the probe by a multimeter, C_s satisfies the following equation:

$$C_s = (a \cdot C_e) / (1 - a) \quad (6)$$

When the electric field between probes and the measured surface is approximately uniform, the effective area S (i.e., spatial resolution) can be determined as follows:

$$S = 4\pi k d C_s \quad (7)$$

where d is the distance between probes and samples, about 3mm. k is the electrostatic force constant, which is approximately $9 \times 10^9 \text{ N} \cdot \text{m}^2/\text{C}^2$.

3 ONLINE MEASUREMENT MODEL OF ELECTROSTATIC PROBE

For the $\pm 320\text{kV}$ GIL tri-post insulator given in [37], a capacitive electrostatic probe measurement model is constructed, as depicted in Fig. 2. The radius of the high voltage conductor (HV-conductor) is 65mm. The radius of the insulator leg area is 40mm and the height is 125mm. The dimensions of the embedded electrode near the grounded enclosure (GND-enclosure) are 56mm in diameter, 39mm in

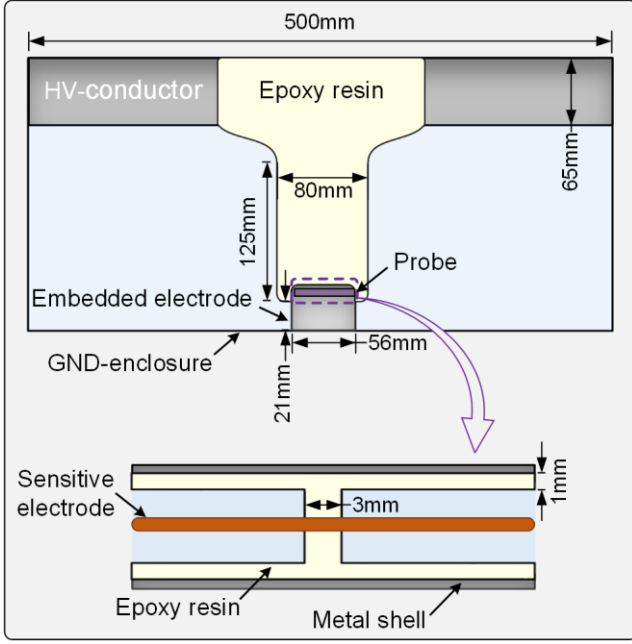


Fig. 2. Online measurement model of the capacitive electrostatic probe for the $\pm 320\text{kV}$ GIL tri-post insulator.

height, and 18mm in depth. The capacitive electrostatic probe is horizontally arranged inside the embedded electrode, perpendicular to the post insulator surface. The thickness of the epoxy resin hollow tube inside the electrostatic probe is 1mm. The epoxy resin in the middle area of the probe is 3mm wide. The material of the sensitive electrode is high conductivity copper. Besides, the insulator material is $\text{Al}_2\text{O}_3/\text{epoxy resin}$. The HV-conductor and GND-enclosure are made of aluminum alloy. The insulation gas is SF_6 . In accordance with the principle of electrostatic induction, the potential φ and the electric field E satisfies the following equations:

$$\nabla \cdot (\varepsilon E) = \rho \quad (8)$$

$$E = -\nabla \varphi \quad (9)$$

where ε is the permittivity. ρ is the space charge density. The relative permittivity of epoxy resin, aluminum alloy, and SF_6 are 4.95, 1×10^5 and 1, respectively.

The electrostatic field around the insulator is subject to the following boundary conditions:

$$\varphi_g = 0 \quad (10)$$

$$\varphi_h = U \quad (11)$$

where φ_g and φ_h are the voltage of the GND-enclosure and the HV-conductor, respectively. U is 320kV.

4 GEOMETRIC OPTIMIZATION OF ELECTROSTATIC PROBE

4.1 Length of sensitive electrode

The surface leakage distance of induced charges on the sensitive electrode varies with the length, as depicted in Fig. 3. The radius of the sensitive electrode is 1.2mm, and the diameter of the probe is 6mm. The surface leakage distance of induced charges on the sensitive electrode increases from 9mm to 29mm when the length rises from 10mm to 50mm. In other words, the leakage distance of the induced charge along the

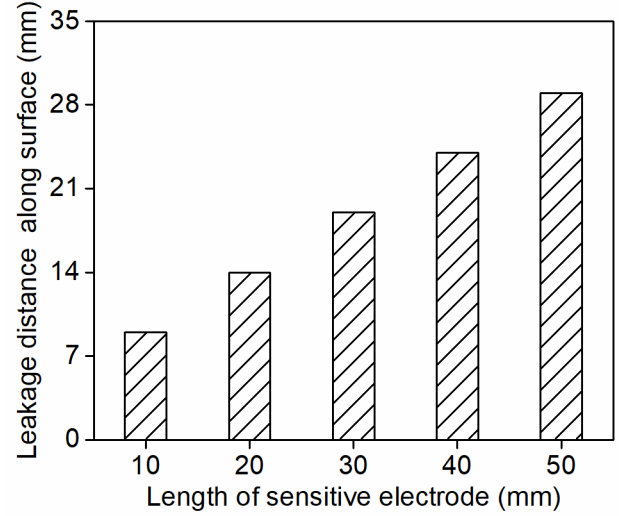


Fig. 3. Surface leakage distance of the induced charge varies with the length of the sensitive electrode.

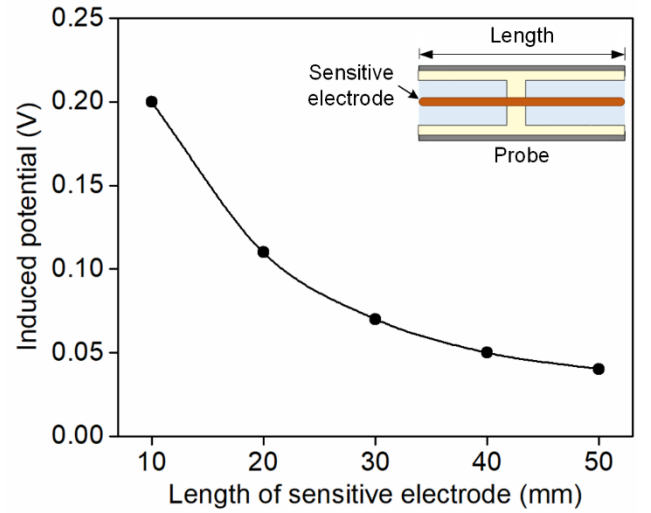


Fig. 4. Induced potential under different lengths of the sensitive electrode.

surface is positively related to the length of the sensitive electrode. Moreover, Fig. 4 shows the induced potential under different lengths of the sensitive electrode. Based on the surface charge distribution of the $\pm 320\text{kV}$ GIL tri-post insulator, the charge density of the insulator in front of the electrostatic probe is assumed to be $30\mu\text{C}/\text{m}^2$. The voltage of the HV-conductor is 320kV. The embedded electrode of post insulators and the shell is grounded. The induced potential of the sensitive electrode is inversely correlated with the length. However, the magnitude of the induced potential is similar and meets the limit of input range for a high input impedance operational amplifier (e.g., $\pm 5\text{V}$ for AD 549LH). Since the leakage of induced charges along the surface in capacitive electrostatic probes is one of the key factors limiting the measurement accuracy, it is necessary to extend the leakage distance of induced charges along the surface to improve the leakage time constant. However, the length of the sensitive electrode is limited by the diameter (56mm) of the embedded electrode. Therefore, the length of the sensitive electrode is a maximum of 50mm.

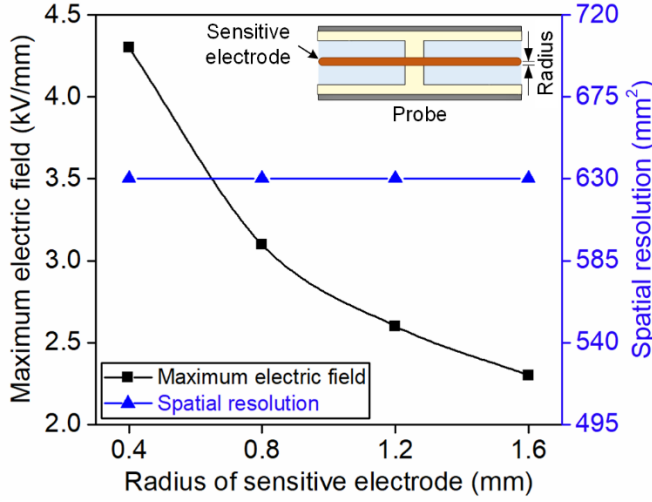


Fig. 5. Variation of the spatial resolution of the probe and the maximum electric field on the sensitive electrode surface with the radius of sensitive electrodes.

4.2 Radius of sensitive electrode

To analyze the impact of sensitive electrode size on the spatial resolution of electrostatic probes, a 3kV voltage is applied to the insulator surface in front of the probe. The embedded electrode, HV-conductor, and GIL enclosure are grounded. According to the electrostatic field equation, Fig. 5 illustrates the spatial resolution of the probe under various radii of sensitive electrodes. The diameter of the probe is 6mm and the length of the sensitive electrode is 50mm. As the radius increases, the spatial resolution remains unchanged, about 630mm². This indicates that the impact of the radius of sensitive electrodes on the spatial resolution can be ignored. This is mainly due to the large distance between the measured surface and the sensitive electrode. Besides, Fig. 5 also shows the change of the maximum electric field on the sensitive electrode surface $E_{\max-s}$ with the radius. $E_{\max-s}$ decreases with increasing the radius. $E_{\max-s}$ reduces from 4.3kV/mm to 2.6kV/mm when the radius is raised to 1.2mm. $E_{\max-s}$ with the radius of 1.6mm is 2.3kV/mm. $E_{\max-s}$ is only reduced by 12% compared to that of the sensitive electrode with the radius of 1.2mm. It is inferred that the radius of sensitive electrodes must be increased to diminish the electric field intensity of the probe. Thus, considering the limitations of mechanical processing on the size, the radius of sensitive electrodes is 1.2mm.

4.3 Diameter of probe

Fig. 6 shows the effect of diameter of electrostatic probes on $E_{\max-s}$ and the spatial resolution. The radius and length of the sensitive electrode are 1.2mm and 50mm, respectively. $E_{\max-s}$ is proportional to the diameter of the probe. For the probe with a diameter of 12mm, $E_{\max-s}$ is as high as 6.9kV/mm, about three times the electric field intensity of probes with a diameter of 6mm. This indicates that the introduction of the probe enhances the distortion of the original electric field as the diameter grows. Moreover, Fig. 6 shows that the spatial resolution of probes remains basically unchanged as the diameter rises from 6mm to 12mm. This means that the effect of the diameter of probes on spatial resolution can also be ignored. Thus, combined with $E_{\max-s}$ and the spatial resolution, the diameter of the electrostatic probe is a minimum of 6mm.

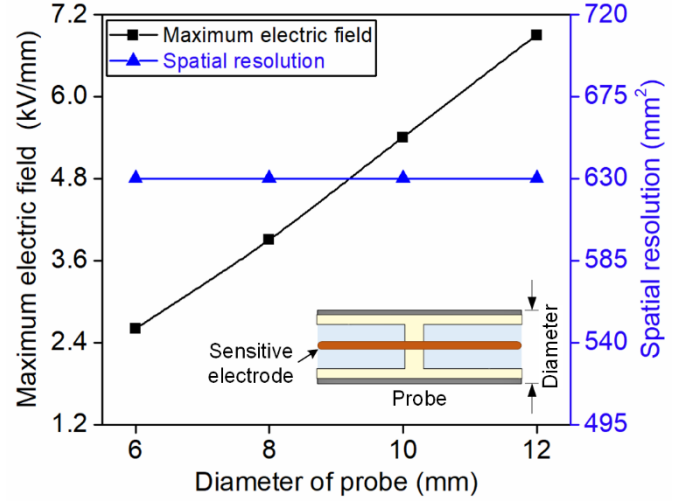


Fig. 6. Maximum electric field on the sensitive electrode and the spatial resolution of the probe under different diameters of the probe.

5 VERIFICATION OF ONLINE MEASUREMENT

5.1 Electric field distribution

Fig. 7 depicts the impact of the arrangement height of electrostatic probes in the tri-post insulator on the maximum electric field on the embedded electrode surface $E_{\max-e}$. The arrangement height of the probe is the vertical distance between its center and the GIL enclosure. The length and radius of the sensitive electrode are 50mm and 1.2mm, respectively. The diameter of the probe is 6mm. As depicted in Fig. 7, $E_{\max-e}$ exhibits an increase from 13kV/mm to 19kV/mm by raising the arrangement height of the probe from 26mm to 29mm. That is to say, $E_{\max-e}$ has a positive correlation with the distance of the probe to the GIL grounded enclosure. Therefore, the minimum arrangement height (26mm) of the probe inside the embedded electrode is selected.

For the arrangement height of 26mm, $E_{\max-e}$ before and after the arrangement of the probe rises from 5kV/mm to 13kV/mm, an increase of nearly three times. Additionally, $E_{\max-e}$ appears at the triple junction of the epoxy resin-SF₆-embedded electrode. It is mainly due to the narrow gas gap at the triple junction. Therefore, to diminish the electric field intensity on the embedded electrode, a gas gap is introduced between the embedded electrode and the insulator. Fig.8 shows the $E_{\max-e}$ under the gas gap of 1mm to 5mm. $E_{\max-e}$ is reduced by about 48% after the introduction of the 1mm gas gap, compared to the case without the gas gap. It can be concluded that the distribution of the electric field on the embedded electrode surface is improved by the introduction of the gas gap. For the gas gap of 2mm and 3mm, $E_{\max-e}$ remains consistent at approximately 5kV/mm. $E_{\max-e}$ is about 4kV/mm as the gas gap increases to 5mm. Since $E_{\max-e}$ before probe arrangement is 5kV/mm, the gas gap should be 2-3mm.

5.2 Spatial resolution

To give the spatial resolution of probes under the online measurement, the induced potential on the sensitive electrode is calculated based on the electrostatic field equation. The

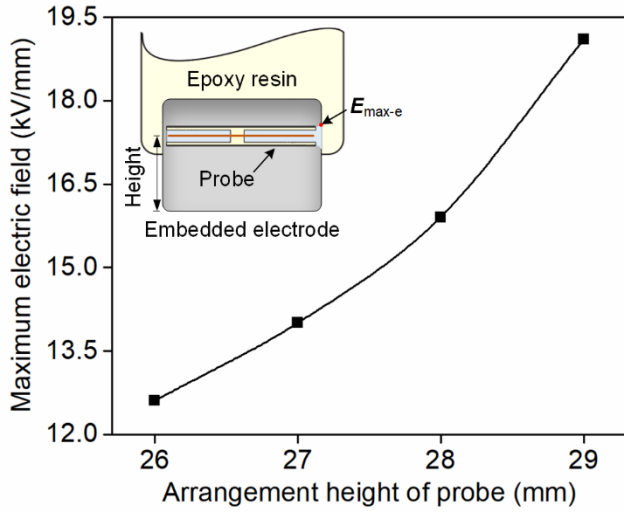


Fig. 7. Effect of arrangement height of electrostatic probes on the maximum electric field of the embedded electrode.

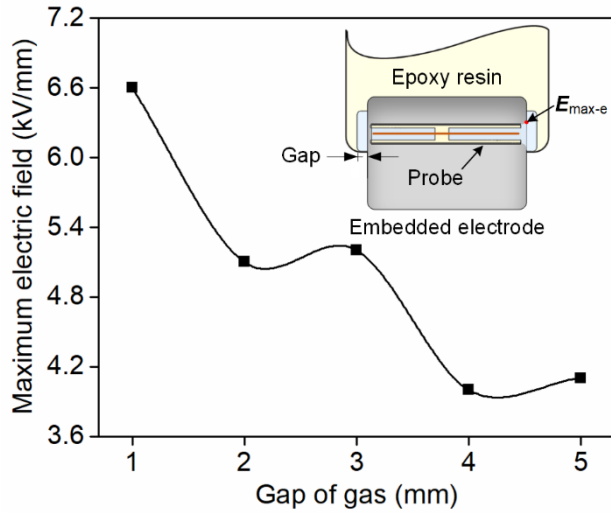


Fig. 8. Variation of the maximum electric field on the embedded electrode surface with gas gaps.

induced potential varies with the effective charged area, as illustrated in Fig. 9. The length and radius of the sensitive electrode are 50mm and 1.2mm, respectively. The diameter of the probe is 6mm. The arrangement height of the probe is 26mm. The induced potential on the sensitive electrode increases rapidly and approaches saturation as the charged area expands. For example, when the charged area is increased from 101mm² to 630mm², the induced potential rises from 1.2V to 2.0V. The growth rate is about 60%. However, the deviation of the induced potential is only 5% when the charged area increases from 630mm² to 2074mm². As a result, the capacitive electrostatic probe has a spatial resolution of 630mm² under the online measurement. The lower spatial resolution is primarily due to the 12mm distance between measured surface and sensitive electrodes. The measurement distance is much greater than the 3mm gap during offline measurement.

5.3 Distribution of induced potential

To verify the online measurement of the surface charge on tri-post insulators, a negative exponential function is utilized

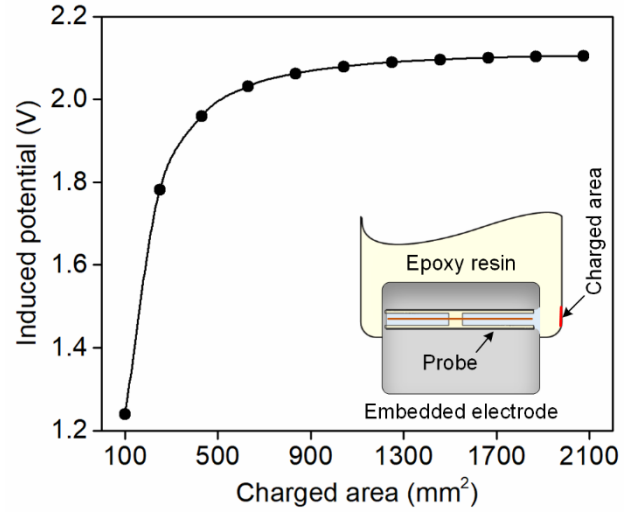


Fig. 9. Distribution of induced potential on the sensitive electrode under different charged areas.

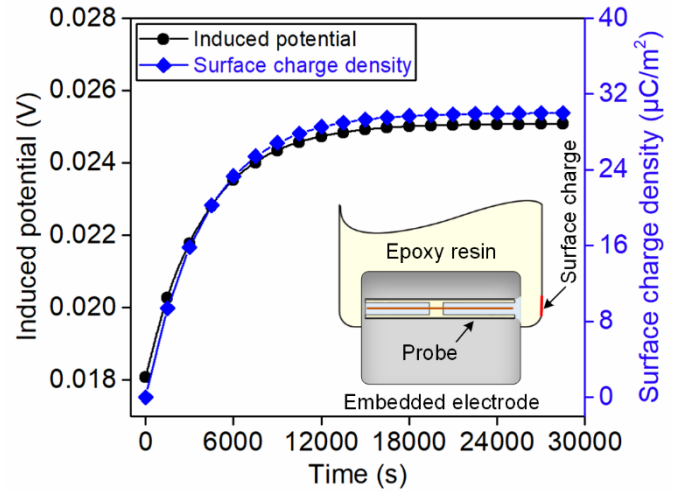


Fig. 10. Changes of surface charge density and induced potential with time.

to define the charge density. In accordance with the law of surface charge accumulation on the DC GIL insulator, the charge density is $30 \times (1 - \exp(-0.00025 \times t)) \mu\text{C}/\text{m}^2$. Furthermore, the charge is located on the insulator surface 630mm² in front of the probe. The change of the calculated induced potential on sensitive electrodes and surface charges with time is depicted in Fig. 10. The length and radius of the sensitive electrode are 50mm and 1.2mm, respectively. The diameter of the probe is 6mm. The arrangement height of the probe is 26mm. The voltage of HV-conductor is 320kV. The embedded electrode and GIL enclosure are grounded. The induced potential on the sensitive electrode increases with the surface charge. Initially, the surface charge is 0. The induced potential is 0.018V due to the effect of the operation voltage. When the time is 15000 seconds, the charge density is 29μC/m² and the induced potential is 0.025V. With further extension of time, the charge density reaches saturation. Meanwhile, the induced potential basically remained unchanged. It means that the distribution of induced potential on the sensitive electrode is generally in agreement with surface charges. Therefore, the induced potential can characterize the surface charge distribution. The capacitive electrostatic probe inside the embedded electrode is

appropriate for online measurements of surface charges on the GIL tri-post insulators.

6 CONCLUSION

This paper presents a model for online measurement of surface charge on $\pm 320\text{kV}$ GIL tri-post insulators by capacitive electrostatic probes. The geometric structure of probes is optimized. The feasibility of the online measurement is verified. The main conclusions are as follows:

1) The leakage distance of the induced charge along the surface is positively related to the length of the sensitive electrode. The increase of insulation distance along the surface is beneficial to improve the leakage time constant of induced charges, thus improving the accuracy of measurement. Furthermore, the diameter of the embedded electrode is only 56mm. Therefore, the length of the sensitive electrode in the electrostatic probe is 50mm.

2) The maximum electric field on the sensitive electrode surface drops with the increase of the radius. As the radius of the sensitive electrode rises, the spatial resolution of the probe remains basically unchanged, about 630mm^2 . After considering the constraints of mechanical processing on the size of the sensitive electrode, the radius is 1.2mm.

3) As the diameter of the probe grows from 6mm to 12mm, the maximum electric field on the sensitive electrode surface increases by nearly three times. That is to say, the introduction of the probe enhances the distortion of the original electric field as the diameter rises. Moreover, the diameter of the probe has a negligible impact on spatial resolution. Hence, the diameter of the probe is only 6mm.

4) For $\pm 320\text{kV}$ GIL tri-post insulators, the maximum electric field on the embedded electrode surface is the smallest when the arrangement height of the capacitive electrostatic probe is 26mm. However, the maximum electric field after the arrangement of the electrostatic probe rises from 5kV/mm to 13kV/mm . Consequently, the gas gap of 2-3mm between the embedded electrode and the insulator is necessary to diminish the electric field intensity. Furthermore, the probe has a spatial resolution of 630mm^2 , and the distribution of the induced potential matches well with the surface charge distribution. This shows that the electrostatic probe is appropriate for online measurement of surface charges on GIL tri-post insulators.

ACKNOWLEDGMENTS

This work was supported by the National Natural Science Foundation of China under Grant 52237007 and 52377143, and the Natural Science Foundation of Hunan Province under Grant 2022JJ20010.

REFERENCES

- [1] Dong, J., Du, B., Liang, H., *et al.*: 'Parameter design of functionally graded materials for tri-post insulator in HVDC GIL under stationary and transient conditions', *IEEE Trans. Dielectr. Electr. Insul.*, 2023, 30, (2), pp. 752-760
- [2] Kong, F., Zhang, S., Lin, H., *et al.*: 'Effects of nanosecond pulse voltage parameters on characteristics of surface charge for epoxy resin', *IEEE Trans. Dielectr. Electr. Insul.*, 2018, 25, (6), pp. 2058-2066
- [3] Gao, Y., Li, Z., Zhao, N., *et al.*: 'Surface charging on Epoxy/ Al_2O_3 nanocomposites under DC voltage superimposed by repetitive pulses', *IEEE Trans. Plasma Sci.*, 2019, 47, (7), pp. 3256-3265
- [4] Li, X., Zhang, G. and Lin, X.: 'Influence of geometry and operation conditions on the surface charge characteristics of DC-GIL spacer', *IET Gener. Transm. Distrib.*, 2022, 16, (9), pp. 1768-1779
- [5] Li, X., Han, S., Wang, W., *et al.*: 'Transient surface charge of SF_6 -filled direct current gas-insulated transmission lines insulator under thermal-electric coupled fields: effects of ambient temperature, load current and gas pressure', *IET Gener. Transm. Distrib.*, 2022, 16, (13), pp. 2688-2700
- [6] Li, X., Wan, M., Wang, W., *et al.*: 'Temperature and electric field distribution of tri-post insulator in DC-GIL based on numerical multiphysics modelling', *IET Gener. Transm. Distrib.*, 2023, 17, (6), pp. 1232-1242
- [7] Li, Y., Zhang, B., Zhou, X., *et al.*: 'Mechanisms of charge-induced surface discharge under positive impulse voltages', *J. Phys. D: Appl. Phys.*, 2024, 57, pp. 175501
- [8] Wang, Z., Wang, Y., Ding, H., *et al.*: 'Modeling of surface trapping effect on charge accumulation pattern at gas-solid interface in DC GIL', *IEEE Trans. Dielectr. Electr. Insul.*, 2024, 31, (1), pp. 466-476
- [9] Zhang, B., Li, Y., Min, D., *et al.*: 'Insight into charge-induced flashover at the gas-solid interface in DC gas-insulated systems', *J. Phys. D: Appl. Phys.*, 2024, 57, pp. 103001
- [10] Luo, Y., Mao, S., Li, Y., *et al.*: 'From surface potential to surface charge: An inversion algorithm for shift-variant system based on Hybrid LBD-Tikhonov method', *IEEE Trans. Instrum. Meas.*, 2023, 72, pp. 1-14
- [11] Tu, Y., Zhou, F., Cheng, Y., *et al.*: 'The control mechanism of micron and nano SiO_2 /epoxy composite coating on surface charge in epoxy resin', *IEEE Trans. Dielectr. Electr. Insul.*, 2018, 25, (4), pp. 1275-1284
- [12] Amer, M., Laninga, J., McDermid, W., *et al.*: 'New experimental study on the DC flashover voltage of polymer insulators: combined effect of surface charges and air humidity', *High Volt.*, 2019, 4, (4), pp. 316-323
- [13] Wang, F., Liang, F., Chen, S., *et al.*: 'Surface charge inversion method on cylindrical insulators based on surface potentials measured online', *IEEE Trans. Dielectr. Electr. Insul.*, 2021, 28, (1), pp. 192-197
- [14] Li, D., Zhang, G., Wang, T., *et al.*: 'Surface charge measurement under AC voltage using active electrostatic probe and controllable phase truncation scheme', *IEEE Trans. Dielectr. Electr. Insul.*, 2020, 27, (2), pp. 684-691
- [15] Li, D., Zhang, G., Hou, Y., *et al.*: 'Charge distribution on polymer insulator surface under AC voltage', *IEEE Trans. Dielectr. Electr. Insul.*, 2019, 26, (5), pp. 1709-1715
- [16] Kindersberger, J. and Lederle, C.: 'Surface charge decay on insulators in air and sulfurhexafluoride-part II: Measurements', *IEEE Trans. Dielectr. Electr. Insul.*, 2008, 15, (4), pp. 949-957
- [17] Wang, Q., Zhang, G. and Wang, X.: 'Characteristics and mechanisms of surface charge accumulation on a cone-type insulator under DC voltage', *IEEE Trans. Dielectr. Electr. Insul.*, 2012, 19, (1), pp. 150-155
- [18] Winter, A. and Kindersberger, J.: 'Transient field distribution in gas-solid insulation systems under DC voltages', *IEEE Trans. Dielectr. Electr. Insul.*, 2014, 21, (1), pp. 116-128
- [19] Kumara, S., Hoque, I. R., Alam, S., *et al.*: 'Surface charges on cylindrical polymeric insulators', *IEEE Trans. Dielectr. Electr. Insul.*, 2012, 19, (3), pp. 1076-1083
- [20] An, Z., Liu, F., Tang, Y., *et al.*: 'Resistance of surface fluorinated epoxy resin to corona discharge in SF_6 gas', *IEEE Trans. Dielectr. Electr. Insul.*, 2016, 23, (6), pp. 3659-3667
- [21] Xie, Q., Liang, S., Fu, K., *et al.*: 'Distribution of polymer surface charge under DC voltage and its influence on surface flashover characteristics', *IEEE Trans. Dielectr. Electr. Insul.*, 2018, 25, (6), pp. 2157-2168
- [22] Xue, J., Wang, H., Liu, Y., *et al.*: 'Surface charge distribution patterns of a truncated cone-type spacer for high-voltage direct current gas-insulated metal-enclosed transmission line/gas-insulated metal-enclosed switchgear', *IET Sci. Meas. Technol.*, 2018, 12, (4), pp. 436-442
- [23] Chen, X., Guan, H., Jiang, T., *et al.*: 'Surface charge dissipation and DC flashover characteristic of DBD plasma treated epoxy resin/ AlN nanocomposites', *IEEE Trans. Dielectr. Electr. Insul.*, 2020, 27, (2), pp. 504-511
- [24] Wang, T., Liu, C., Li, D., *et al.*: 'Nano ZnO /epoxy coating to promote surface charge dissipation on insulators in DC gas-insulated systems', *IEEE Trans. Dielectr. Electr. Insul.*, 2020, 27, (4), pp. 1322-1329
- [25] Li, C., Lin, C., Jun, H., *et al.*: 'Novel HVDC spacers by adaptively controlling surface charges - Part I: Charge transport and control strategy', *IEEE Trans. Dielectr. Electr. Insul.*, 2018, 25, (4), pp. 1238-1247
- [26] Han, Y., Li, S. and Min, D.: 'Nonlinear conduction and surface potential decay of Epoxy/ SiC nanocomposites', *IEEE Trans. Dielectr. Electr.*

- Insul., 2017, 24, (5), pp. 3154-3164
- [27] Zhang, L., Lin, C., Li, C., *et al.*: 'Gas-solid interface charge characterisation techniques for HVDC GIS/GIL insulators', *High Volt.*, 2020, 5, (2), pp. 95-109
 - [28] Du, Q., Zhang, Q., Wu, Z., *et al.*: 'Surface charge distribution on DC basin-type insulator', *IEEE Trans. Dielectr. Electr. Insul.*, 2019, 26, (1), pp. 17-25
 - [29] Li, C., Zhang, C., Lv, J., *et al.*: 'China's 10-year progress in DC gas-insulated equipment: From basic research to industry perspective', *iEnergy*, 2022, 1, (4), pp. 400-433
 - [30] Zhou, H., Ma, G., Wang, C., *et al.*: 'Review of charge accumulation on spacer of gas insulated equipment at DC stress', *CSEE J. Power Energy*, 2019, 6, (3), pp. 496-517
 - [31] Tschentscher, M. and Franck, C. M.: 'Microscopic charge provision at interfaces of gas-insulated (HVDC/HVAC) systems', *IEEE Trans. Dielectr. Electr. Insul.*, 2018, 25, (4), pp. 1186-1194
 - [32] Zhang, B., Li, X., Wang, T., *et al.*: 'Surface charging characteristics of GIL model spacers under DC stress in C_4F_7N/CO_2 gas mixture', *IEEE Trans. Dielectr. Electr. Insul.*, 2020, 27, (2), pp. 597-605
 - [33] Faircloth, D. C. and Allen, N. L.: 'High resolution measurements of surface charge densities on insulator surfaces', *IEEE Trans. Dielectr. Electr. Insul.*, 2003, 10, (2), pp. 285-290
 - [34] Ma, J., Tao, F., Ma, Y., *et al.*: 'Quantitative analysis on the influence of surface charges on flashover of insulators in SF_6 ', *IEEE Trans. Dielectr. Electr. Insul.*, 2021, 28, (1), pp. 274-281
 - [35] Qi, B., Gao, C., Liu, S., *et al.*: 'Surface charge distribution on GIS insulator under DC/AC voltage', *IEEE Trans. Dielectr. Electr. Insul.*, 2017, 24, (5), pp. 3173-3181
 - [36] Wang, F., Qiu, Y., Pfeiffer, W., *et al.*: 'Insulator surface charge accumulation under impulse voltage', *IEEE Trans. Dielectr. Electr. Insul.*, 2004, 11, (5), pp. 847-854
 - [37] Liang, F., Fan, X., Hu, J., *et al.*: 'Surface charging physics of the basin insulator in ± 320 kV gas-insulated transmission lines', *IEEE Trans. Dielectr. Electr. Insul.*, 2024, 31, (3), pp. 1654-1656